Volume 1 | Number 2 | April 2014 | Pages 83–192

Environmental Science Nano

rsc.li/es-nano

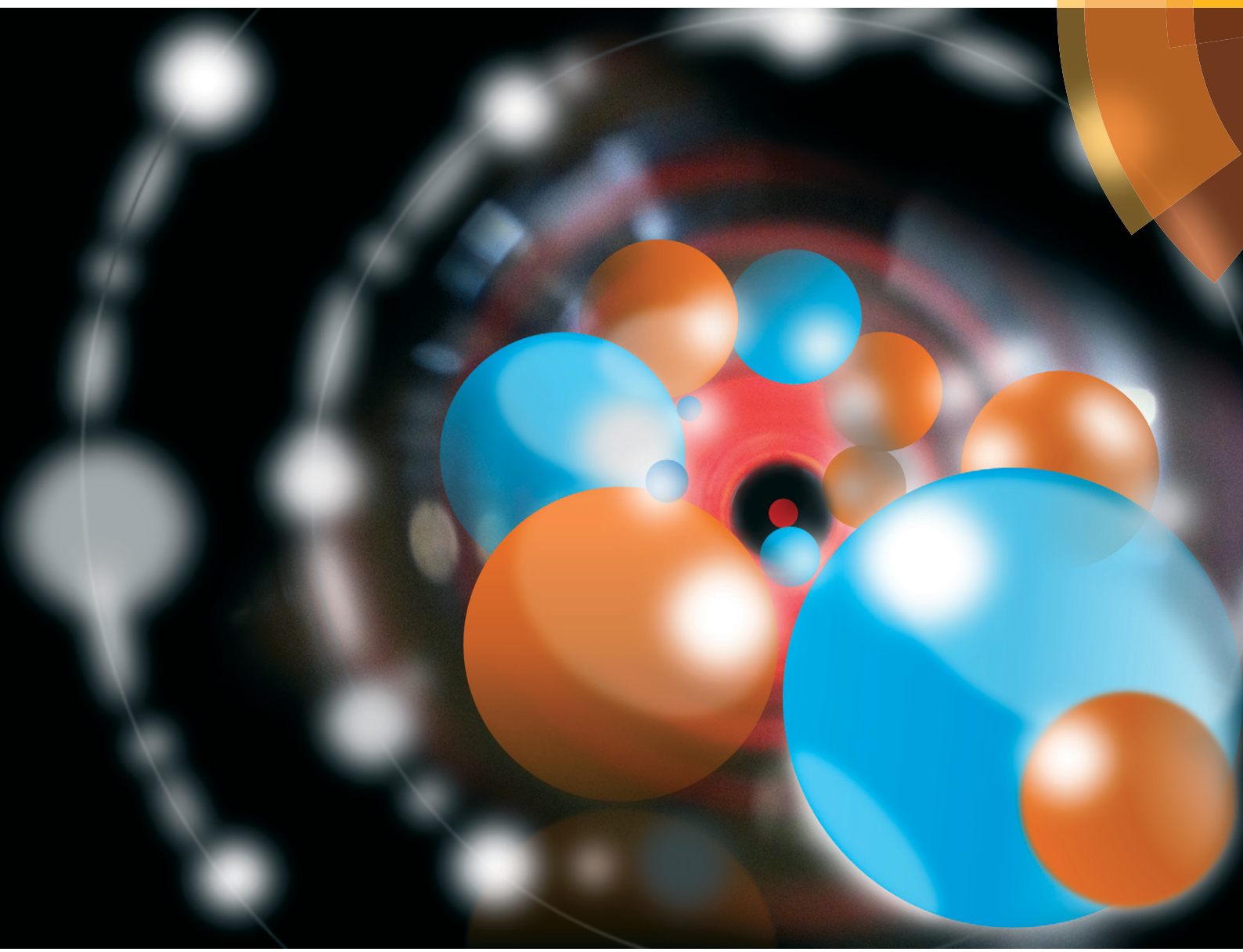

ISSN 2051-8153

ROYAL SOCIETY OF CHEMISTRY

PAPER
Linsey C. Marr *et al.*
Characterization of particle emissions and fate of nanomaterials during incineration

Environmental Science Nano

PAPER

View Article Online
View Journal | View Issue

Characterization of particle emissions and fate of nanomaterials during incineration†

Cite this: *Environ. Sci.: Nano*, 2014, **1**, 133

Eric P. Vejerano, Elena C. Leon, Amara L. Holder and Linsey C. Marr*

Received 12th November 2013,
Accepted 9th January 2014

DOI: 10.1039/c3en00080j

rsc.li/es-nano

As the use of nanotechnology in consumer products continues to grow, it is inevitable that some nanomaterials will end up in the waste stream and will be incinerated. Through laboratory-scale incineration of paper and plastic wastes containing nanomaterials, we assessed their effect on emissions of particulate matter (PM) and the effect of incineration on the nanomaterials themselves. The presence of nanomaterials did not significantly influence the particle number emission factor. The PM size distribution was not affected except at very high mass loadings (10 wt%) of the nanomaterial, in which case the PM shifted toward smaller sizes; such loadings are not expected to be present in many consumer products. Metal oxide nanomaterials reduced emissions of particle-bound polycyclic aromatic hydrocarbons. Most of the nanomaterials that remained in the bottom ash retained their original size and morphology but formed large aggregates. Only small amounts of the nanomaterials (0.023–180 mg g^{-1} of nanomaterial) partitioned into PM, and the emission factors of nanomaterials from an incinerator equipped with an electrostatic precipitator are expected to be low. However, a sustainable disposal method for nanomaterials in the bottom ash is needed, as a majority of them partitioned into this fraction and may thus end up in landfills upon disposal of the ash.

Nano impact

As more engineered nanomaterials are incorporated into consumer products, and ultimately discharged into the environment, it is certain that some will be incinerated. The fate and behavior of nanomaterials during incineration and their effects on the properties of the emitted particulate matter are largely unknown. This study is important in understanding the flow of nanomaterials into the environment and their potential impacts.

Introduction

As the widespread use of nanotechnology-based consumer products continues to grow, it is inevitable that some nanomaterials will end up in the waste stream and will be incinerated. The amount of nanomaterials expected to be incinerated annually is estimated to be 4 metric tons in Switzerland,[1,2] 440 metric tons in the US,[1,2] and 8600 metric tons globally.[3] Incineration could modify the size, morphology, structure, and composition of the nanomaterial as well as the properties of the airborne particulate matter (PM) that is generated, some of which may be emitted to the atmosphere. These changes may alter the toxicity of the nanomaterial itself and the toxicity of the PM.

Currently, little is known about how nanomaterials interact with waste during end-of-life treatment such as incineration. To date, only a few studies have investigated the effects of incineration on nanomaterials and pollutant emissions. The addition of nanomaterials in surrogate waste and plastics increases the emissions of certain combustion by-products and decreases emissions of others, including toxic polycyclic aromatic hydrocarbons (PAHs) and polychlorinated dibenzofurans/dioxins (PCDD/Fs).[4–6] The ultimate fate of nanomaterials in incinerators and potential for exposure to them depend on how they partition between the bottom ash and the PM during combustion. Ceria nanoparticles introduced into a full-scale municipal solid waste (MSW) incinerator are unchanged by the process, and most of them remain in the bottom ash.[7] Whether other nanomaterials behave similarly to ceria is currently unknown.

The toxicity of PM depends on its mass and number concentration, particle size, surface area, and chemical composition, although understanding of the relationship is not yet

Civil and Environmental Engineering Department, Virginia Tech, 411 Durham Hall, Blacksburg, VA 24061, USA. E-mail: lmarr@vt.edu; Fax: +540 231 7916; Tel: +540 231 6071

† Electronic supplementary information (ESI) available: Active surface area, metal/metal oxide/C_{60} concentration of the control waste and spiked waste, particle size and particle number emissions, deposition on aerosol chamber, CO_2 mixing ratio, EDX maps, and propagated uncertainty and coagulation coefficient equations. See DOI: 10.1039/c3en00080j

complete. Scarce data exist on the properties of PM produced by nanowaste incineration, and these properties may change as the PM passes through different combustion zones, where it may be subject to condensation and aggregation. Temperature strongly affects the amount and size of nanomaterials that are released as PM during incineration.[8]

Nanomaterials added to a polymer composite have been shown to influence combustion by-products. Emissions of PM are lower in number but larger in size when carbon nanotubes are added to the composite.[9] Nanomaterials incorporated into a nanocomposite may potentially be released during combustion in a form that may or may not differ from the original one. For instance, single-walled carbon nanotubes incorporated in polymer matrices are released unmodified as isolated and bundled fibers,[10] while some nanomaterials experience physico-chemical modification during combustion.[9]

In this study, which is a companion to our paper on combustion by-product emissions,[6] we characterized PM emitted from the incineration of paper and plastic wastes containing nanomaterials in a laboratory-scale incineration system. Additionally, we investigated the changes in the size and morphology of the nanomaterials themselves. We focused on silver, NiO, TiO_2, ceria, C_{60}, Fe_2O_3, and quantum dots because they are produced and used in large volumes[1,2] and/or represent a cross-section of different types of nanomaterials.

Results

Partitioning of nanomaterials

We have investigated the incineration of nanomaterials spiked as a suspension into surrogate waste. Results may differ for some nanomaterials that are embedded in consumer products (*e.g.*, composites). During incineration, nanomaterials could partition into PM in the exhaust or into bottom ash. The majority of the nanomaterials were found in the bottom ash (Table 1). Walser *et al.*[7] reported a similar result for the incineration of ceria in a full-scale incinerator. C_{60} was an exception that was detected in the PM but not in the bottom ash. We did not detect C_{60} in PM from the unspiked control waste;[6] thus, the C_{60} must have persisted through incineration.

The higher PM emission factors at lower loadings (0.1 wt% *v.* 1 wt% *v.* 10 wt%) suggest that the waste may become saturated with nanomaterials at higher loadings, and additional nanomaterials may not be incorporated well into the waste matrix. We were not able to close the mass balance for the nanomaterials because of thermophoretic loss (movement of particles from a hotter region to a cooler region due to differences in gaseous diffusivities, and thus in bombardment of the particles by gas molecules, along the temperature gradient)[11] of the ash to the reaction tube during its removal from the furnace, which we estimate to range from 10% to 25%. Also, we did not measure the volatile metal chlorides formed. Additionally, adhesion of nanomaterials to the container wall during sample preparation and during transfer of the waste to the sample boat contributed to losses in mass.

Particle size and particle number emission factors

We measured the PM size and emission factor to determine the effect of addition of nanomaterials to waste undergoing incineration. The PM fell mainly within the accumulation mode; the median diameter for waste containing 0.1 wt% nanomaterials was 385–398 nm (Fig. 1A), not significantly different from that of control waste that did not contain any nanomaterials. The addition of 1 wt% nanomaterials to the waste (not shown) also did not result in any significant change in the median diameter. However, for samples containing 10 wt% nanomaterials, the median particle size shifted to a significantly smaller diameter of 310–339 nm. At this loading, there was no significant difference across the different types of nanomaterials.

The emission factors, in terms of particle number emitted per mass of waste burned, ranged from 1.9×10^{13} to 4.5×10^{13} particles g^{-1} (Fig. 1B). In most cases, the emission factor

Table 1 Emission factors of nanomaterials in the PM and bottom ash fractions

	Emission factor (mg g^{-1} of nanomaterial)					
	0.1 wt%		1 wt%		10 wt%	
Nanomaterial	PM	Bottom ash	PM	Bottom ash	PM	Bottom ash
Silver	21	260	1.3	240	0.44	290
NiO	24	620	[a]	770	[a]	1100
TiO_2	1.9	58	0.044	110	0.035	750
Ceria	nd	57	nd	380	0.023	820
C_{60}[c]	nd	nd	180	nd	68	nd
Fe_2O_3	[a]	320	[a]	670	[a]	1000
CdSe QD[b]	6.6	15	5.6	57	0.040	400

[a] Metal concentration for unspiked waste is higher than with nanomaterial. [b] Measured as Cd. [c] Measured by HPLC, nd not detected. The relative standard deviation for six of the samples (two samples at each mass loading) that were run in duplicate was less than 12%. All values are corrected for the metal/metal oxide/C_{60} concentration in the control waste. Table S2 and S3 (ESI†) list the concentrations in the unspiked control waste and the spiked waste, respectively.

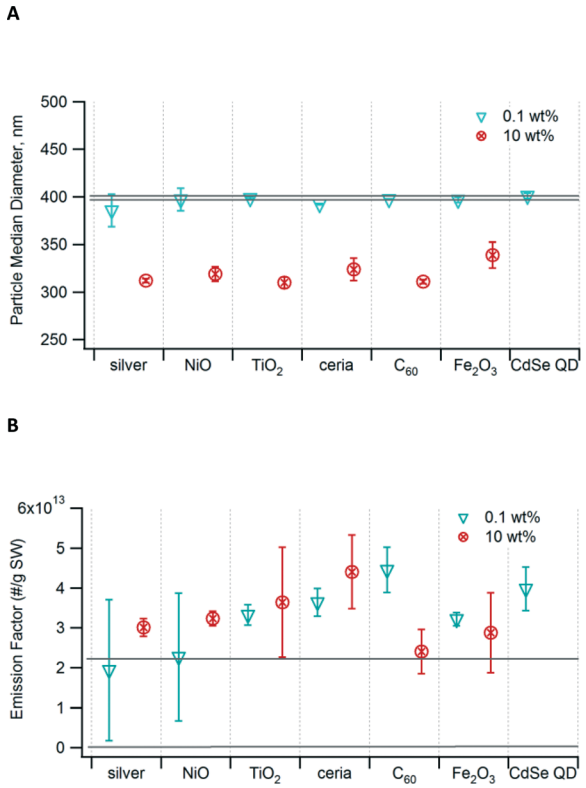

Fig. 1 (A) Median diameter of PM generated from incineration of waste containing nanomaterials. (B) Particle emission factor as number per gram of surrogate waste (SW) incinerated. The area bounded by the two grey lines in each graph is the 95% confidence interval for the unspiked control waste. Error bars show the 95% confidence interval. Data for 10 wt% CdSe QD are not available. Values are indicated in Table S4 in the ESI.†

for waste containing nanomaterials was higher than that of the control, but the differences were not significant. While the mass loading of nanomaterials varied by a factor of 100 (0.1 wt% *v.* 10 wt%), the resulting emission factors varied by no more than a factor of ~2 for any given nanomaterial. At high mass loading, the nanomaterials clumped together and were not well incorporated into the waste matrix.

Active surface area, *s*-PAH, and combustion efficiency

Active surface area, defined as that accessible to a molecule diffusing toward the particle is another important parameter in assessing the toxicity of particles. Moshammer and Neuberger[12] have suggested that the active surface area is a better indicator of particles' toxicity than is particle mass or number concentration, as surface area correlates well with symptoms of respiratory distress. Generally, the active surface area of the PM exhaust decreased with higher loading of the nanomaterial and was higher than that of the control only at 0.1 wt% loading (Table S1†). The active surface area concentration in the diluted exhaust followed this trend with respect to type of nanomaterial: NiO > C_{60} > ceria, TiO_2 > Fe_2O_3, CdSe QD, and silver.

Among the numerous classes of hazardous by-products emitted from combustion sources, PAHs and PCDD/Fs may pose the greatest environmental and health concerns. Results of our earlier study of PAH speciation suggest that some nanomaterials affect the formation of the more volatile 2–3 ring PAH species.[6]

We measured emissions of total surface-bound PAHs (*s*-PAH) adsorbed on particles. We calculated emission factors as the amount of *s*-PAH emitted per mass of waste burned and the enhancement factor as the ratio of the emission factor of the sample containing the nanomaterial compared to the emission factor of the unspiked control waste. The enhancement factors were <1 for most of the nanomaterials. This means that the emission factor was lower for waste containing nanomaterials than for waste without them. Only the samples with 0.1 wt% NiO, 0.1 wt% C_{60}, and 1 wt% CdSe QD had enhancement factors >1, although only the latter was significantly different from 1. Metal oxide nanomaterials—NiO, TiO_2, ceria, and Fe_2O_3—resulted in a decrease in *s*-PAH enhancement factor as the mass loading of the nanomaterial increased (Fig. 2). The 0.1 wt% and 1 wt% Fe_2O_3 nanoparticles had the smallest enhancement factors compared to the other nanomaterials. Even at low mass loading of the nanomaterial, Fe_2O_3 had the smallest enhancement factor (*i.e.*, largest reduction in *s*-PAH emissions) compared to other nanomaterials at similar mass loading. Additionally, the decrease in *s*-PAH enhancement factor for C_{60} was consistent with our earlier finding that at higher nanomaterial loading, chlorine-containing fuel fragments from PVC interact well with C_{60}.[6] Only silver promoted the formation of *s*-PAH with increased mass loading of the nanomaterial.

For most samples, *s*-PAH and active surface area emissions were correlated. Shifts in the ratio of *s*-PAH to active surface area may indicate that the nanomaterial has affected pollutant formation. The values presented in Fig. 3 were calculated as the ratio of the *s*-PAH (ng m^{-3}) to active surface area (mm^2 m^{-3}) in the exhaust for each nanomaterial. The ratios for all samples and every mass loading of the nanomaterial tended to cluster between 50 and 150 (Region II,

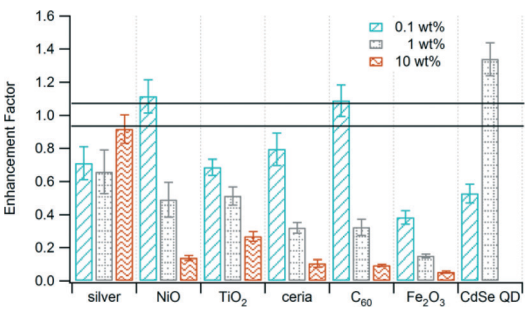

Fig. 2 Enhancement factor of *s*-PAH from the incineration of waste containing various nanomaterials at different mass loading. The area bounded by the lines is the enhancement factor for the unspiked control waste. Error bars are the propagated uncertainty (eqn (1), ESI†). Data for 10 wt% CdSe QD are not available.

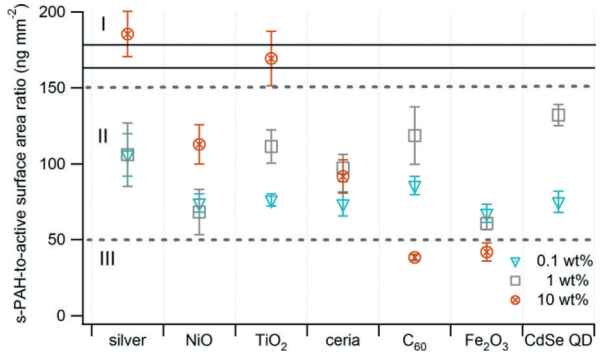

Fig. 3 Ratio of *s*-PAH to active surface area. Error bars are the propagated uncertainty (eqn (1), ESI†). The solid black lines delineate the ratio of *s*-PAH to active surface area for the unspiked control waste. Data for 10 wt% CdSe QD are not available.

Fig. 3) except for the 10 wt% samples, which were distributed across all three regions. The ratio increased with an increase in mass loading of the nanomaterial for Ag, NiO, and TiO_2, and it decreased for C_{60} and Fe_2O_3. One confounding factor is that the present study is based on photoemission measurement, which is most sensitive to 4–6 ring PAH species on the particle surface.

As nanomaterials have different surface areas and physico-chemical properties (*i.e.*, catalytic, band gap), they might absorb oxygen and enhance or reduce combustion efficiency to varying degrees. Differences in CO_2 emissions between the waste containing nanomaterials and the control were not statistically significant. CO_2 concentrations in the undiluted exhaust ranged from ~13 000 to ~16 000 ppm of dry air (Fig. S2†). Assuming that the carbon contents of the PVC, polyethylene, and paper (estimated to contain pure cellulose) were 38%,[13] 86%,[13] and 44% respectively, suggests that half of the carbon content in the waste was oxidized to CO_2, <4% to PM, and the rest to CO and gas-phase products of incomplete combustion. However, typically CO accounts for only 10–20% of carbon in the waste.[4,14] The carbon contents of the surrogate waste materials (bottles, gloves, and paper) are likely to be lower than that of pristine polyethylene, PVC, and cellulose. If so, the amount of CO_2 emitted would account for >50% of the carbon. As the differences in CO_2 emissions between samples were small, the effect of nanomaterials on combustion efficiency cannot be distinguished. However, since PAHs are products of incomplete combustion, the ratio of *s*-PAH to CO_2 concentration may be a better indicator. For all samples containing metal oxide nanomaterials, the ratio decreased with an increase in mass loading of the nanomaterial, suggesting enhanced combustion of the waste (Table 2). The addition of C_{60} resulted in an increase in CO_2 emissions and a decrease in the enhancement factor for *s*-PAH with an increase in mass loading (Fig. 2). It is inaccurate, however, to determine the effect of C_{60} on combustion efficiency by the *s*-PAH-to-CO_2 ratio only, as C_{60} is also oxidized to CO_2. Our earlier study indicates that indeed C_{60} reduces PAH emissions.[6]

Table 2 *s*-PAH-to-CO_2 ratio in exhaust[a]

	s-PAH/CO_2 ratio (ng mg^{-1})		
Nanomaterial	0.1 wt%	1 wt%	10 wt%
Silver	0.97	1.0	1.4
NiO	1.5	0.66	0.20
TiO_2	0.95	0.76	0.39
Ceria	1.2	0.47	0.14
C_{60}	1.5	0.21	0.12
Fe_2O_3	0.53	0.20	0.069
CdSe QD	0.77	—	—

[a] *s*-PAH/CO_2 ratio for the control is 1.0 ng mg^{-1}.

Persistence of nanomaterials in the bottom ash

The extent to which combustion and the waste matrix affect the size and morphology of the nanomaterial itself is relatively unknown. It is expected that metal-containing nanomaterials will retain their size and morphology, whereas carbon-based nanomaterials will be easily oxidized. This was not the case however, as presented above for C_{60}. Results of our electron microscopy analysis revealed that for most of the nanomaterials in the bottom ash, there were no substantial changes in size and morphology of the primary particles (Fig. 4). Most of the particles aggregated, however. For ceria, we found aggregates consisting of smaller nanoparticles that were similar to the original unburned nanoparticles. Ceria, TiO_2, and Fe_2O_3 nanoparticles aggregated and appeared to be encapsulated. TiO_2 and Fe_2O_3 retained their ~20 nm size and spherical morphology. The exception was NiO, which did not aggregate and was not encapsulated. The original unburned NiO nanoparticles were spherical in shape, but after incineration some cubic particles along with some rods formed. Additionally, the incinerated NiO particles were much larger than the unburned ones. The metallic nanoparticles such as CdSe QD became larger, as did silver to some extent (Fig. 4). We found larger particles containing Cd and Zn, which may have originated from CdSe QD and formed Cd–O, as evidenced by the very strong oxygen signal in Fig. 5R. Given the small size of the original quantum dots, <~10 nm, they are likely to melt and form larger particles. However, we still observed some smaller CdSe QD nanoparticles that resembled the original unburned nanoparticles. Silver nanoparticles did not aggregate and generally retained their size and spherical morphology, but some particles larger than the initial ones were also observed.

Some metal chlorides and sulfides formed. The EDX maps (Fig. S3†) for some of the samples revealed a chlorine signal, suggesting that the nanomaterial reacted with the chlorine in PVC. The EDX map for the TiO_2 particles correlated to some extent with sulfur and chlorine (Fig. S3†).

For the PM fraction, we could not find any nanoparticles during EDX analysis, despite the bulk analysis (Table 1) indicating significant presence of the nanomaterials. Obviously, they must be there, but substantially greater resources would be required to locate them. Nevertheless, we hypothesize that

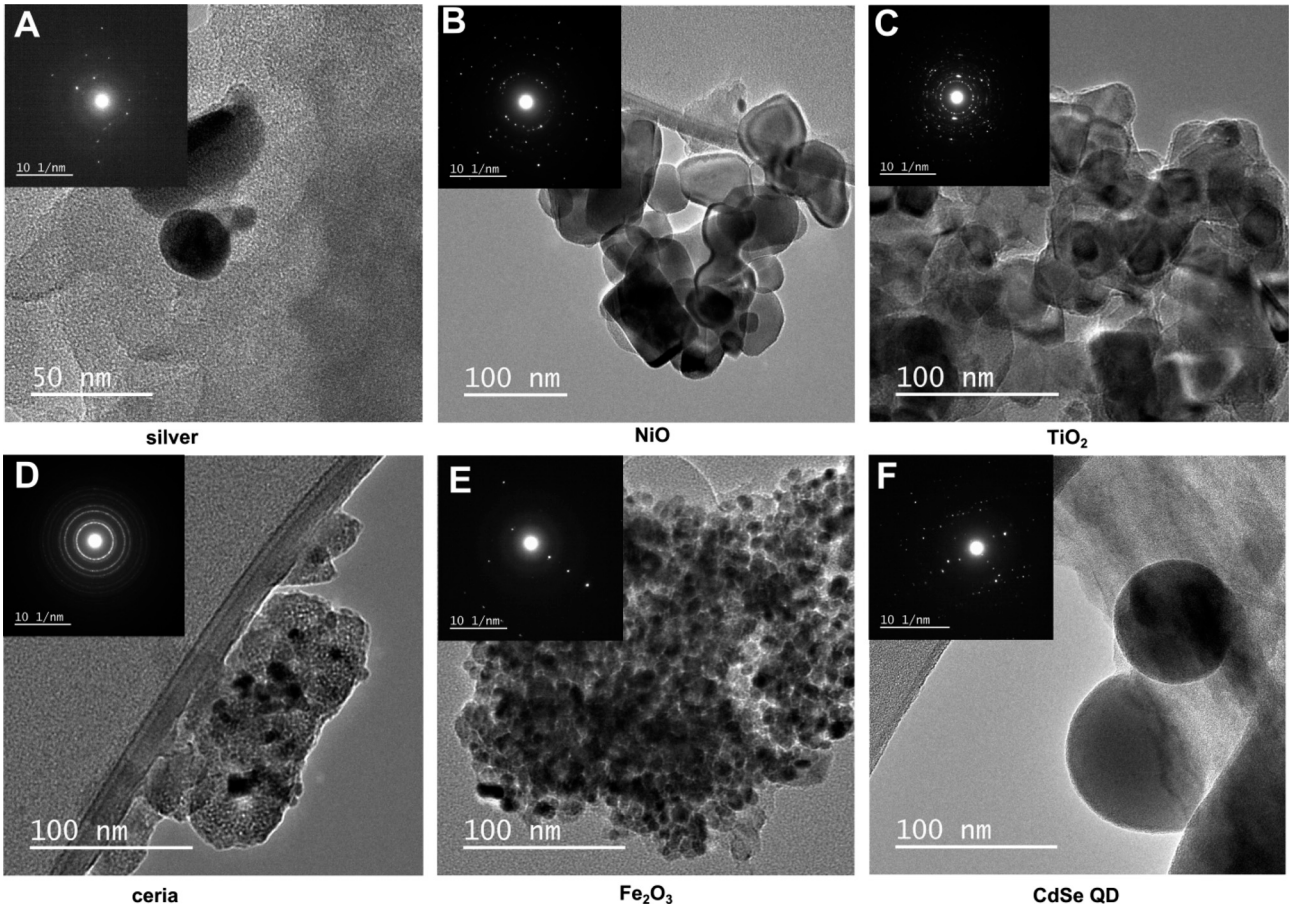

Fig. 4 Representative TEM image of nanoparticles in the bottom ash fraction. (A) Isolated silver nanoparticles. (B) NiO particles were larger than the unburned nanoparticles and did not aggregate. (C) TiO_2 nanoparticles retained their size but appear to be encapsulated and formed aggregates. (D) Aggregate of ceria nanoparticles. (E) Fe_2O_3 nanoparticles also retained their size but aggregated. (F) CdSe QD nanoparticles formed highly spherical nanoparticles larger than the original unburned nanomaterial. The insets are the diffraction patterns for the particles.

the nanomaterials in the PM fraction might be modified more than those in the bottom ash because of their reactions with multitudes of by-products as they entered the different combustion zones.

When we incinerated greyish NiO nanoparticles, the ash became green, suggesting that some fraction of the nanoparticles may have undergone stoichiometric conversion.[15] The electron diffraction pattern of ceria (Fig. 4D) matched that of the original nanoparticles, suggesting the absence of phase transition consistent with the reports in the literature. The measured *d*-spacing of 2.90 Å in the [101] plane was close to the *d*-spacing of anatase TiO_2. The measured *d*-spacing of 2.51 Å agreed with the *d*-spacing for rutile (2.49 Å), confirming phase transition of TiO_2 during incineration. The measured *d*-spacing for Fe_2O_3, however, did not agree with any of the *d*-spacing values in the literature for either γ-Fe_2O_3 or α-Fe_2O_3. However, the *d*-spacing of 5.78 Å might have indicated formation of Fe_3O_4 (5.91 Å). While the X-ray counts for oxygen were lower and did not coincide well with the particle containing silver (Fig. 5C), the measured *d*-spacing of 2.01 Å agreed with the distance for an Ag–O system (2.04 Å).[16] Additionally, oxygen chemisorbed on the surface of silver was suggested by the *d*-spacing of 4.01 Å, which was close to the *d*-spacing of 4.09 Å for such system.[16] The *d*-spacing of 2.74 Å for the ash containing CdSe QD was close to the *d*-spacing of 2.71 Å[17] in the [111] plane, supporting what we observed in the EDX analysis as formation of CdO.

Discussion

Assessing the partitioning and persistence of nanomaterials during incineration is important, as these two factors affect the transport, fate, toxicity, and exposure potential of the nanomaterials in combustion systems. The extent to which nanomaterials are affected by the waste matrix, whether they preferentially partition into PM or bottom ash, and any transformations of the nanomaterials themselves have remained largely unknown for most nanomaterials. In a full-scale incinerator, nanomaterials can partition to other compartments such as wastewater during the treatment and removal of flue gases, bottom ash, and PM including fly ash. This study has shown that at 0.1 wt% loading of nanomaterials in waste, there was a 55–250% increase in particle number emission factors, no change in size, and a 20–60% decrease in *s*-PAH

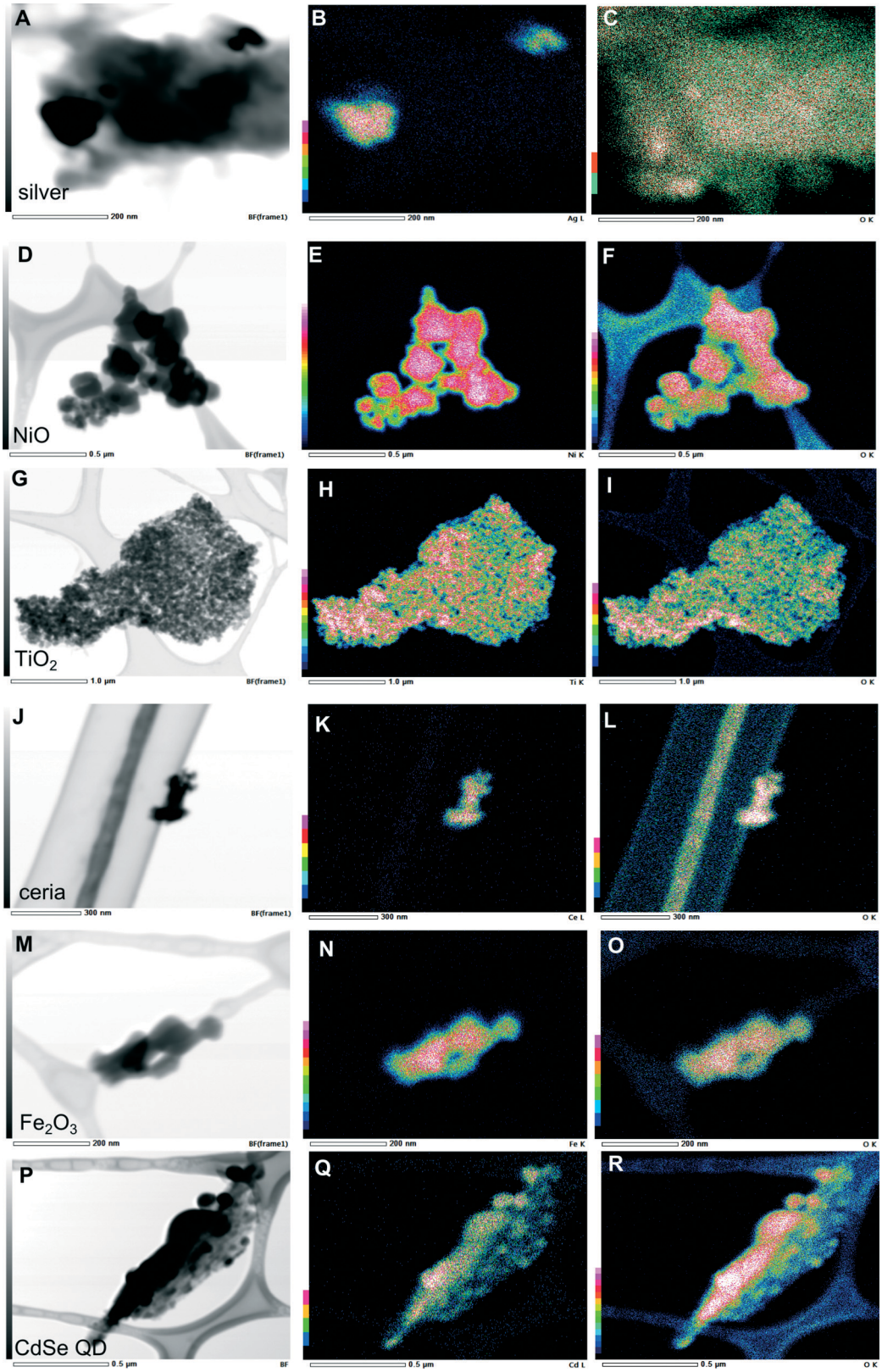

Fig. 5 Brightfield images of particles from waste containing (A) silver, (D) NiO, (G) TiO_2, (J) ceria, (M) Fe_2O_3, and (P) CdSe QD. EDX maps of the metals of interest whose brightfield images are shown on the left: (B) silver, (E) NiO, (H) TiO_2, (K) ceria, (N) Fe_2O_3, and (Q) CdSe QD nanomaterials. (C), (F), (I), (L), (O), and (R) are the oxygen signals suggesting the preservation or formation of the metal oxide system. Brighter colors indicate higher X-ray counts.

emission factors compared to the control. It appears that the nanomaterial has a greater chance of getting into PM for Ag, NiO, TiO_2, and CdSe QD at lower mass loading as the PM emission factor is higher at lower mass loadings. Clumping of nanomaterials at high mass loading would lead to the nanomaterials not burning with the waste and thus losing the opportunity to become PM.

C_{60} is interesting because it is the only nanomaterial that partitions more into the PM than the bottom ash in this study. In isolation, C_{60} is completely oxidized at ~500 °C,[18] so in theory, it should not survive incineration. We suspect that the spiking method—dosing the waste with C_{60} in solution and then allowing the solvent to evaporate—results in the C_{60} coating and effectively diffusing into the waste. This treatment could protect the C_{60} from oxidation. Thus, studies of the combustion of nanomaterials in isolation may not be indicative of their fate during incineration, when they are part of a complex matrix of waste. Additionally, layers of combustion-generated species (*e.g.*, PAHs) may have coated the C_{60} and protected it from further oxidation.

Growth of particles in combustion systems depends on nucleation, aggregation, agglomeration, and heterogeneous reaction with gas-phase products.[18,19] Our results indicate that the median size of PM in combustion exhaust is nearly 100 nm smaller at a nanomaterial loading of 10 wt% compared to 0.1 wt%. The different combustion by-products emitted from the waste at the two mass loadings might explain the size difference, as heterogeneous reactions of combustion by-products and their subsequent condensation on particle surfaces are important determinants of particle size.[18,19] We attribute the larger particle size associated with 0.1 wt% loading of nanomaterials to high emissions of benzo[*k*]fluoranthene; its emissions are much lower at 10 wt% loading of nanomaterials.[6] Among the larger PAHs, only benzo[*k*]fluoranthene was formed at high concentrations, and condensation of it onto particles would increase their size. For samples containing 10 wt% nanomaterials, we attribute the smaller particle size to the formation of volatile metal chlorides (formed from the reaction with the chlorine in PVC) and metal oxides. These volatile species could homogenously nucleate in the post-combustion zone and become nuclei for condensing gas-phase species.[19,20]

The presence of nanomaterials seems to affect emissions of combustion by-products, resulting in a higher particle number emission factor compared to the control. The aerosol processes, however, remained unperturbed by either the type of the nanomaterial or by the mass loading. This is expected given the fact that only a small fraction of the nanomaterials partition into PM. The clustering of PAH-to-active-surface-area ratios within a particular region suggests that most of the nanomaterials influence the formation of the 4–6 ring particle-bound PAH species similarly. This result is consistent with our earlier study on PAH speciation showing that most of the 4–6 ring PAH species, except benzo[*k*]fluoranthene, are insensitive to both the mass loading and the type of the nanomaterials.[6] The smaller active surface area at higher mass loading may be due to the smaller particle size combined with only a small change in the particle number emission factor.

The decrease in *s*-PAH emissions with addition of metal oxides agrees with reports in the literature that ceria nanoparticles that are used as a diesel-fuel additive can reduce PM emissions in the accumulation mode.[21] Most metal oxides can serve as catalysts and therefore would behave similarly to the ceria nanoparticles in reducing emissions. The presence of surface-active oxygen species and surface anionic vacancies, oxidation state of the metal, and character of the metal itself[22] might be responsible for the decreased *s*-PAH emissions for the waste containing metal oxide nanomaterials. Also, metals in their higher oxidation state, as can be found in combustion systems, are more catalytic.[22] Redox cycling of metals, as demonstrated for ceria, contributes to their enhanced catalytic activity.[23] The enhanced *s*-PAH emissions for silver may be a result of less favorable redox cycling between Ag^0 and Ag^+ as compared with other metal oxide nanomaterials. However, the formation of surface oxygen species as indicated by the electron diffraction pattern and other physico-chemical properties may contribute as well. The oxidation of metallic silver consumed a fraction of the supplied oxygen that was available for combustion of the waste, resulting in reduced combustion efficiency.[6] The enhancement factor for CdSe QD might suggest that their small size or the physico-chemical properties of core–shell metals may be a factor in catalyzing higher emissions of *s*-PAH.

Although incineration may not necessarily modify the morphology of some nanomaterials, subtle structural changes such as phase transition may occur. Phase transitions may result in different crystal structures and changes in the nanomaterials' physico-chemical properties, and hence affect their fate, transport, and environmental impacts. For instance, the β–α phase transition of Ag_2S (which may be the form of silver nanoparticles entering incinerators[24]) results in dramatic changes in both ionic and electrical conductivities by several orders of magnitude.[25] Additionally, structural changes (*e.g.*, rutile *v.* anatase TiO_2) can alter the mechanism of their toxicity.[26] Phase transition for some bulk crystalline compounds occurs well below the temperature used in typical incinerators, less so for nanomaterials given their high surface energies. For instance bulk γ-Fe_2O_3 becomes α-Fe_2O_3 at ~500 °C.[27] The initiation transition temperature for anatase TiO_2 to its more thermodynamically stable rutile form ranges from 520 °C to 850 °C[28,29] depending on size, and the transition occurs rapidly above 730 °C.[30]

In this study, the original unburned nanomaterials are all face-centered cubic, except ceria which is a cubic fluorite and TiO_2 which is tetragonal. The complex electron diffraction patterns for some nanomaterials compared to the original nanoparticles indicate that other phases might form during incineration and that chloride species might facilitate phase transition.[31] It appears that the species produced by incineration and the incineration itself may introduce structural defects and complicate the diffraction patterns of the

nanomaterials. However, ceria is an exception, in that up to its melting point (bulk ceria, ~2300 °C), it produces high amounts of structural vacancy without undergoing phase transition.[32] Formation of cubic structures in NiO indicates the dominant role of chloride species. The abundance of chloride species from PVC in the incinerator might facilitate the formation of cubic NiO nanoparticles, as chloride ions promote the synthesis of cubic nanocrystals.[31] The formation of large clusters suggests that nanomaterials begin melting at 850 °C in the presence of the waste matrix. The formation of other phases suggests that some nanomaterials, specifically those with melting points and initiation transition temperatures close to those used in typical MSW incinerators, are subject to various physico-chemical transformations.

Based on the emission factors presented in Table 1, we have estimated the amount of nanomaterials that could be emitted in an incinerator's flue gas. We consider the most commonly used air pollution control devices: electrostatic precipitator, wet/dry scrubbers, and fabric filter (baghouse). Traditional wet scrubbers and cyclones are not considered, as they are expected to be ineffective for nanoparticles.[33]

First, we calculate the size-resolved emission factor of each nanomaterial (mass emitted per mass dosed into the waste) as the product of the uncontrolled emission factor and the penetration efficiency of that particle size through the device:

$$E_c(d) = \sum E_u(d)(1 - \eta(d))$$

where $E_c(d)$ and $E_u(d)$ are the controlled and the uncontrolled emission factors, respectively, and $\eta(d)$ is the removal efficiency for particle size d. For an electrostatic precipitator we assume a removal efficiency of 50%,[34] for a wet electrostatic or ionizing wet scrubber 70%,[35] and for a fabric filter 99.9%[36] for particles of diameter 300–400 nm. We use this size as it is the median particle size (Fig. 1A) and the hardest to remove, and therefore represents a worst-case scenario. This size range encompasses both engineered nanoparticles and incidental nanoparticles that were created by incineration of the waste. The emissions of nanomaterials from an incinerator equipped with a fabric filter are predicted to range from as low as 2.3×10^{-5} mg g^{-1} and to as high as 1.8×10^{-1} mg g^{-1} of the dosed nanomaterials (Table 3). These emission factors are at least two orders of magnitude lower compared to those for an incinerator equipped with an electrostatic precipitator or a wet electrostatic or ionizing wet scrubber. Using the controlled emission factors, we estimate that a typical MSW incinerator equipped with an electrostatic precipitator and with a daily feed capacity of 100 metric tons would emit 0.13–1.5 kg yr^{-1} of nanomaterials depending on the type, in the stack flue gas, if we assume that 13%[2] of the waste contains 0.1 wt% nanomaterials. This value is specific to Switzerland, and global variations in the type and fraction of the waste are to be expected. In the unlikely case in which 100% of the waste contained 0.1 wt% nanomaterials, the emission factors for the nanomaterials would be 1–12 kg yr^{-1}. For the types of nanomaterials and the type of waste considered here, the amount emitted into the atmosphere from incinerators equipped with air pollution control devices represents only 0.021% to 0.25% of the yearly input of nanomaterials entering incinerators for the scenario described above.

The largest stream of nanomaterials to the environment from incineration will be the bottom ash. These nanomaterials are likely to end up in landfills. In the scenario described above, the nanomaterial input to landfills is estimated to range from 70 to 2900 kg yr^{-1} and from 550 to 22 000 kg yr^{-1} if 13% and 100% of the waste contained 0.1 wt% of the nanomaterials, respectively, depending on the type of nanomaterial. This amount is three orders of magnitude higher than the amount emitted in the flue gas. The significant losses in mass in our experiments may result in underestimation of the calculated emissions of nanomaterials into landfills and the atmosphere.

Conclusions

The amount of nanomaterials in the waste stream will continue to grow, and some of them are certain to be incinerated. Our study has demonstrated that most of the nanomaterials remained in the bottom ash and only a small amount partitioned into the PM. C_{60} was an exception that appeared to be protected from oxidation by the waste matrix, and a significant amount of it was detected in PM.

Table 3 Controlled emission factor of nanomaterials in electrostatic precipitator, fabric filter, and wet electrostatic or ionizing wet scrubber

	Controlled emission factor, $E_c(d)$, (mg g^{-1} nanomaterial)								
	Electrostatic precipitator			Fabric filter			Wet electrostatic or ionizing wet scrubber		
Nanomaterial	0.1 wt%	1 wt%	10 wt%	0.1 wt%	1 wt%	10 wt%	0.1 wt%	1 wt%	10 wt%
Silver	10	0.65	0.22	0.021	0.0013	0.00044	6.3	0.39	0.130
NiO	12	[a]	0	0.024	[a]	[a]	7.2	[a]	[a]
TiO_2	0.95	0.022	0.018	0.0019	0.000044	0.000035	0.57	0.013	0.010
Ceria	[a]	[a]	0.012	[a]	[a]	0.000023	[a]	[a]	0.0069
C_{60}	[a]	90	34	[a]	0.18	0.068	[a]	54	20
Fe_2O_3	[a]	[a]	[a]	[a]	[a]	[a]	[a]	[a]	[a]
CdSe QD	3.3	2.8	0.02	0.0066	0.0056	0.000040	2.0	1.7	0.012

[a] Emission factor for the control waste was greater than the waste containing nanomaterials.

Whether other carbon-based nanomaterials will behave like C_{60} demands attention, as they are being incorporated into many composite materials.

At mass loadings present in many consumer products, nanomaterials did not affect the size distribution of PM emitted from nanowaste incineration. The particle number emission factor of the PM exhaust was higher in the presence of the nanomaterials but was not significantly different compared to the nanomaterial-free waste. The type and mass loading of the nanomaterials influenced combustion efficiency. Metal oxides and C_{60} decreased the emissions of particle-bound PAHs and enhanced combustion efficiency, whereas a metallic nanomaterial (silver) resulted in an increase in emissions. The presence of surface active sites and the highly catalytic properties of metal oxide nanomaterials may be responsible for the effect.

Nanomaterials in the bottom ash retained their size and morphology, and some nanoparticles became encapsulated. TiO_2, ceria, and Fe_2O_3 formed large aggregates while silver, NiO, and CdSe QD did not. The size of the nanomaterials increased, possibly due to their interactions with components of the waste.

The low level of nanomaterials present in PM coupled with the high removal efficiency of air pollution control devices, especially fabric filters if present, implies that the amount released into the atmosphere from an incinerator is expected to be low. However, development of a viable option for the disposal of the enriched nanomaterials in the bottom ash is warranted. However, because of the considerable losses in mass to container walls in our experiments, our estimates of the amounts released to the environment may represent a lower bound. These nanomaterials may be aerosolized during transport and disposal to landfills. They may be subject to environmental processing such as atmospheric and photocatalytic reactions with pollutants and may be transported from their source and leached to groundwater. The potential for release of some of the encapsulated nanomaterials may be low, as conditions for their release are not expected to occur in landfills. However, some nanomaterials may remain loose and become a potential source for exposure. Exposure to combustion by-products, PM, and bottom ash that contain nanomaterials remains a concern in countries where open burning is prevalent.

This study represents only a preliminary step in understanding the transformation, fate, and effects of nanomaterials that are subject to incineration. Results of this laboratory-scale study are informative, but they cannot readily be extended to account for the fate and behavior of nanomaterials in a full-scale incinerator. Turbulent conditions in incinerators may effectively aerosolize nanomaterials that are released from the waste matrix, thereby increasing their partitioning to PM. Therefore, a full-scale incineration study is still needed. The results are useful to update data currently used in models of nanomaterial flows in the environment, as these models often rely on data obtained from nanomaterials' bulk counterparts.

Experimental

Nanomaterials and surrogate waste preparation

We investigated seven nanomaterials: anatase TiO_2 (TiO_2, particle size <25 nm, specific surface area 200–220 $m^2\ g^{-1}$, purity ≥ 99.7%), NiO (NanoAmor, 10–20 nm, 50–80 $m^2\ g^{-1}$, ≥99.8%), silver (coated with poly(vinyl pyrrolidone), NanoAmor, 30–50 nm, 5–10 $m^2\ g^{-1}$, ≥99.5%), ceria (NanoAmor, 15–30 nm, 30–50 $m^2\ g^{-1}$, ≥99.9%), Fe_2O_3 (<30 nm, ≥99%), CdSe/ZnS quantum dots (CdSe QD, <10 nm), and C_{60} (SES Research, ≥99.8%). We dispersed the nanomaterials in ethanol, except for C_{60}, which we dissolved in toluene.

We produced samples of surrogate waste containing 50 mg each of paper, polyethylene cut from plastic bottles, and poly(vinyl chloride) (PVC) from PVC gloves, chosen to be representative of routine medical and laboratory wastes.[37] We spiked the waste with a single type of nanomaterial at 0.1 wt%, 1 wt%, or 10 wt%. We chose the lowest loading of 0.1 wt% to be representative of the nanomaterial content in many consumer nanoproducts[38] and we chose the higher loadings of 1 wt% and 10 wt% to ensure the discrimination of effects on emissions. All measurements were made in duplicate with the exception of the partitioning study, in which we analysed only six samples (two samples at each mass loading) in duplicate.

Particle concentration and size distribution

We incinerated the spiked waste samples (0.1 wt% and 10 wt%) in a cylindrical furnace at 850 °C with 1.0 L min^{-1} of air flowing through it, as described previously.[6] Anti-static conductive tubing routed the exhaust through a 64 L polyethylene chamber into which we introduced particle-free clean air at 1.0 L min^{-1} to dilute the PM. We collected the PM until no more visible exhaust came out of the reactor (~20 s). We assumed that plug flow conditions prevailed and only particle-free air exited the chamber through the outflow on the opposite end; the volume of exhaust introduced was ~0.3 L, less than 1% of the chamber's total volume. The PM in the chamber was then stirred with a fan. After 15 s, we measured the particle size distribution using a scanning mobility particle sizer (SMPS, TSI 3936NL) for particles of mobility diameter 14 nm to 720 nm and an aerodynamic particle sizer (APS, TSI 3321) for particles of aerodynamic diameter 720 nm to 5 μm for 2 min and 1 min, respectively. We merged the resulting size distributions from the SMPS and APS using TSI DataMerge™ software and plotted them as mobility diameter *v.* particle number.

To quantify particle losses due to deposition on the chamber wall, we used a constant output atomizer (TSI 3076) to generate aerosol from a 6.70 mM aqueous NaCl solution. We monitored the decay in total particle number concentration for 30 min at 3 min intervals between measurements. We used an initial total particle number concentration of $8.9 \times 10^5\ cm^{-3}$ to minimize coagulation. Losses in the total particle number emission factor over the sample collection period

due to deposition to the chamber walls was 2% ± 0.1% (calculated from the data presented in Fig. S1†).

During the 30 min interval, the particle median diameter shifted from 110 nm to 138 nm while the geometric standard deviation shifted only slightly from 1.54 to 1.58. Hence, we used the equation derived by Lee and Chen[39] (eqn (2), ESI†) for calculating the coagulation coefficient. We estimated particle losses due to coagulation during the 30 s sample collection time to be 1%. We deemed losses due to deposition and coagulation to be negligible and did not correct for them.

Active surface area, surface-bound PAH (*s*-PAH), and CO_2 emissions

For measurement of active surface area and *s*-PAH, we sampled the exhaust through a venturi tube at 0.303 L min^{-1} with dilution air at 1.0 L min^{-1}, and we added a secondary dilution flow to create a final dilution factor of 9. In some cases, we added a third dilution system to reduce the concentration to within the dynamic range of the instruments. A diffusion charger (DC, DC 2000, EcoChem) measured the active surface area of the particles and a photoemission aerosol sensor (PAS, PAS 2000 CE, EcoChem) measured the *s*-PAH. The principles behind the DC and PAS are described by Marr *et al.*[40] and Thornhill *et al.*[41] The instruments recorded data at 30 s and 10 s intervals, respectively, and we averaged the measurements over a 5 min window. The measurement of *s*-PAH by the PAS should be considered semi-quantitative. In addition to measuring active surface area and *s*-PAH for the samples already described, we also measured them for samples containing individual components of the surrogate waste (*i.e.*, paper by itself, polyethylene by itself, and PVC by itself).

We measured CO_2 in the chamber with an infrared absorption analyzer (LI-COR 7000).

Bulk analysis of nanomaterials

We collected the PM onto polytetrafluoroethylene filters (PTFE, diameter 40 mm, pore size 1 μm) for assessment of the partitioning of the nanomaterials between the PM and the bottom ash. We sonicated the filters in 5 mL of dichloromethane for 5 min to extract the PM. For samples containing metallic nanomaterials, we digested 1 mL of the PM extract in 5 mL HNO_3 : HCl (1 : 3 *v*/*v*), HNO_3 : H_2SO_4 (1 : 1 *v*/*v*) or HNO_3 : HF : H_2O_2 (1 : 1 : 1 *v*/*v*) at 100 °C for 3 h. We filtered the samples through a nylon filter (diameter 4 mm, pore size 0.2 μm), diluted with 2% HNO_3 solution, and measured the concentration using inductively coupled plasma-mass spectrometry (ICP-MS, Thermo Electron X-series, detection limit 0.5 ppb). For measurement of C_{60} in PM, we evaporated the solvent from 1 mL of the PM extract, added 1 mL of toluene, sonicated for 30 min, filtered, and then measured the concentration using high-performance liquid chromatography (HPLC, Hewlett-Packard 1090).

We recovered the bottom ash from the sample boat with 5 mL of dichloromethane and then evaporated the solvent at room temperature. We digested the bottom ash in the same way as the PM, and we measured the concentration using ICP-MS. To extract C_{60} in the bottom ash, we dispersed the sample in toluene and extracted in the same way as for the PM, and we measured the concentration using HPLC.

Analysis of nanomaterials by electron microscopy

To determine whether incineration affected the size and morphology of the nanomaterials, we focused on the waste containing the highest concentration, 10 wt% of nanomaterials, to facilitate their detection by transmission electron microscopy (TEM), except that for CdSe QD we used a loading of 1 wt% due to difficulties in completely removing the solvent with this material. We used a micro-analysis particle sampler (MPS-3, California Instrument) to deposit the diluted PM onto amorphous, carbon-coated, 200 mesh, gold TEM grids. The MPS-3 collected samples for 30 s at a flow rate of 0.5 L min^{-1}. The MPS-3 consists of a three-stage impactor; the last stage has a cut-off diameter (d_{50}) of 50 nm.

Following incineration and allowing for cooling, we withdrew the bottom ash from the reactor and suspended it in methanol, sonicated for 1 h, diluted 100×, and drop-casted it onto a 200 mesh, lacey-carbon-coated copper TEM grid. To remove hydrocarbons that would have interfered with analysis, we heated the samples under vacuum at 120 °C for 3 h. The samples were stored under vacuum or nitrogen until analysis. We used a JEM 2100 TEM (JEOL Corporation) operated at 200 kV and equipped with an energy dispersive X-ray (EDX) spectrometer and a diffractometer. We also acquired TEM images and diffraction patterns of the pristine unburned nanomaterials that were prepared using the same procedure as for the bottom ash.

Acknowledgements

This work was funded by the US Environmental Protection Agency under a Science to Achieve Results grant (83485601). The Center for Environmental Implications of Nanotechnology (National Science Foundation EF-0830093) and the Institute for Critical Technologies and Applied Science at Virginia Tech also provided support. We acknowledge use of the facilities and the assistance of Dr. Christopher Winkler at the Nanoscale Characterization and Fabrication Laboratory at Virginia Tech.

References

1 F. Gottschalk, T. Sonderer, R. W. Scholz and B. Nowack, *Environ. Sci. Technol.*, 2009, **43**, 9216–9222.
2 N. C. Mueller and B. Nowack, *Environ. Sci. Technol.*, 2008, **42**, 4447–4453.
3 A. A. Keller and A. Lazareva, *Environ. Sci. Technol. Lett.*, 2014, **1**, 65–70.
4 R. Font, A. Galvez, J. Molto, A. Fullana and I. Aracil, *Chemosphere*, 2010, **78**, 152–159.
5 S. H. Kim, S.-Y. Ahn and S.-Y. Kwak, *Appl. Catal., B*, 2008, **79**, 296–305.

6 E. P. Vejerano, A. L. Holder and L. C. Marr, *Environ. Sci. Technol.*, 2013, **47**, 4866–4874.
7 T. Walser, L. K. Limbach, R. Brogioli, E. Erismann, L. Flamigni, B. Hattendorf, M. Juchli, F. Krumeich, C. Ludwig, K. Prikopsky, M. Rossier, D. Saner, A. Sigg, S. Hellweg, D. Gunther and W. J. Stark, *Nat. Nanotechnol.*, 2012, **7**, 520–524.
8 S. Derrough, G. Raffin, D. Locatelli, P. Nobile and C. Durand, *J. Phys. Conf. Ser.*, 2013, **429**, 012047.
9 C. Motzkus, C. Chivas-Joly, E. Guillaume, S. Ducourtieux, L. Saragoza, D. Lesenechal, T. Mace, J. M. Lopez-Cuesta and C. Longuet, *J. Nanopart. Res.*, 2012, **14**, 1–17.
10 J. Bouillard, B. R. Mili, D. Moranviller, A. Vignes, O. Le Bihan, A. Ustache, J. S. Bomfim, E. Frejafon and D. Fleury, *J. Nanopart. Res.*, 2013, **15**, 1–11.
11 *Aerosol Measurement: Principles, Techniques, and Applications*, ed. P. Kulkarni, P. A. Baron and K. Willike, 3rd edn, John Wiley & Sons, Hoboken, New Jersey, 2011.
12 H. Moshammer and M. Neuberger, *Atmos. Environ.*, 2003, **37**, 1737–1744.
13 Z. Wang, J. Wang, H. Richter, J. B. Howard, J. Carlson and Y. A. Levendis, *Energy Fuels*, 2003, **17**, 999–1013.
14 Y. Zhang, Q. Li, A. Meng and C. Chen, *Waste Manage. Res.*, 2011, **29**, 294–308.
15 S. J. Teichner and J. A. Morrison, *Trans. Faraday Soc.*, 1955, **51**, 961–966.
16 A. Michaelides, M. L. Bocquet, P. Sautet, A. Alavi and D. A. King, *Chem. Phys. Lett.*, 2003, **367**, 344–350.
17 C. Vogt, G. P. Knowles, S. L. Y. Chang and A. L. Chaffee, *J. Mater. Chem. A*, 2013, **1**, 10962–10971.
18 M. Wohlers, A. Bauer and T. Belz, *Preprint Paper Am. Chem. Soc. Div. Fuel Chem.*, 1996, **41**, 108–112.
19 A. Miller, G. Ahlstrand, D. Kittelson and M. Zachariah, *Combust. Flame*, 2007, **149**, 129–143.
20 J. Seinfield and S. Pandis, *Atmospheric Chemistry and Physics: From Air Pollution to Climate Change*, John Wiley and Sons, Hoboken, NJ, 2006.
21 H. Jung, D. B. Kittelson and M. R. Zachariah, *Combust. Flame*, 2005, **142**, 276–288.
22 I. E. Wachs, *Catal.Today*, 2005, **100**, 79–94.
23 B. Solsona, T. García, R. Murillo, A. Mastral, E. Ntainjua Ndifor, C. Hetrick, M. Amiridis and S. Taylor, *Top. Catal.*, 2009, **52**, 492–500.
24 B. Kim, C.-S. Park, M. Murayama and M. F. Hochella Jr., *Environ. Sci. Technol.*, 2010, **44**, 7509–7514.
25 S. Kashida, N. Watanabe, T. Hasegawa, H. Iida, M. Mori and S. Savrasov, *Solid State Ionics*, 2003, **158**, 167–175.
26 K. Hirakawa, M. Mori, M. Yoshida, S. Oikawa and S. Kawanishi, *Free Radical Res.*, 2004, **38**, 439–447.
27 S. Kachi, K. Momiyama and S. Shimizu, *J. Phys. Soc. Jpn.*, 1963, **18**, 106–116.
28 N. Satoh, T. Nakashima and K. Yamamoto, *Sci. Rep.*, 2013, 3.
29 M. Pal, J. Garcia Serrano, P. Santiago and U. Pal, *J. Phys. Chem. C*, 2006, **111**, 96–102.
30 A. W. Czanderna, C. N. R. Rao and J. M. Honig, *Trans. Faraday Soc.*, 1958, **54**, 1069–1073.
31 Z. Xu, C. Shen, Y. Tian, X. Shi and H. J. Gao, *Nanoscale*, 2010, **2**, 1027–1032.
32 W. C. Chueh and S. M. Haile, *Philos. Trans. R. Soc. London, Ser. A*, 2010, **368**, 3269–3294.
33 A. L. Holder, E. P. Vejerano, X. Zhou and L. C. Marr, *Environ. Sci.: Processes Impacts*, 2013, **15**, 1652–1664.
34 M. Strand, J. Pagels, A. Szpila, A. Gudmundsson, E. Swietlicki, M. Bohgard and M. Sanati, *Energy Fuels*, 2002, **16**, 1499–1506.
35 H. Zhao and C. G. Zheng, *Chem. Eng. Technol.*, 2008, **31**, 1824–1837.
36 G. Buonanno, L. Stabile, P. Avino and E. Belluso, *Waste Manage.*, 2011, **31**, 2253–2262.
37 N. Deng, Y. Zhang and Y. Wang, *Waste Manage.*, 2008, **28**, 1572–1580.
38 A. G. Oomen, M. Bennink, J. G. M. van Engelen and A. J. A. M. Sips, *Nanomaterials in Consumer Products: Detection, Characterization and Interpretation*, National Institute for Public Health and the Environment, 2011, http://www.rivm.nl/bibliotheek/rapporten/320029001.pdf.
39 K. W. Lee and H. Chen, *Aerosol Sci. Technol.*, 1984, **3**, 327–334.
40 L. C. Marr, K. Dzepina, J. L. Jimenez, F. Reisen, H. L. Bethel, J. Arey, J. S. Gaffney, N. A. Marley, L. T. Molina and M. J. Molina, *Atmos. Chem. Phys.*, 2006, **6**, 1733–1745.
41 D. A. Thornhill, B. de Foy, S. C. Herndon, T. B. Onasch, E. C. Wood, M. Zavala, L. T. Molina, J. S. Gaffney, N. A. Marley and L. C. Marr, *Atmos. Chem. Phys.*, 2008, **8**, 3093–3105.